Applied and Computational Mechanics 6 (2012) 93–106

Energy transformation and flow topology in an elbow draft tube

D. Štefan[a,*], P. Rudolf[a], A. Skoták[b], L. Motyčák[b]

[a] *Faculty of Mechanical Engineering, Brno University of Technology, Technická 2896/2, 616 69 Brno, Czech Republic*
[b] *CKD Blansko Engineering, a.s., Čapkova 2357/5, 678 01 Blansko, Czech Republic*

Received 20 January 2012; received in revised form 30 April 2012

Abstract

Paper presents a computational study of energy transformation in two geometrical configurations of Kaplan turbine elbow draft tube. Pressure recovery, hydraulic efficiency and loss coefficient are evaluated for a series of flow rates and swirl numbers corresponding to operating regimes of the turbine. These integral characteristics are then correlated with local flow field properties identified by extraction of topological features. Main focus is to find the reasons for hydraulic efficiency drop of the elbow draft tube.

Keywords: draft tube, efficiency, pressure recovery, flow topology

1. Introduction

Draft tubes are diffusers placed at the outlet of the hydraulic turbine runner, see Fig. 1. Their main purpose is transformation of the residual kinetic energy into pressure energy with maximum efficiency. Although geometrically relatively simple the internal flow can be quite complex due to adverse pressure gradient, possible boundary layer separation, swirling and streamline curvature. The elbow draft tubes are usually used for a vertical arrangement of Kaplan turbines. The most problematic part of the draft tube with negative influence on flow properties is the elbow. Paper summarizes results of a computational study of energy transformation in two geometrically different configurations of Kaplan turbine elbow draft tube.

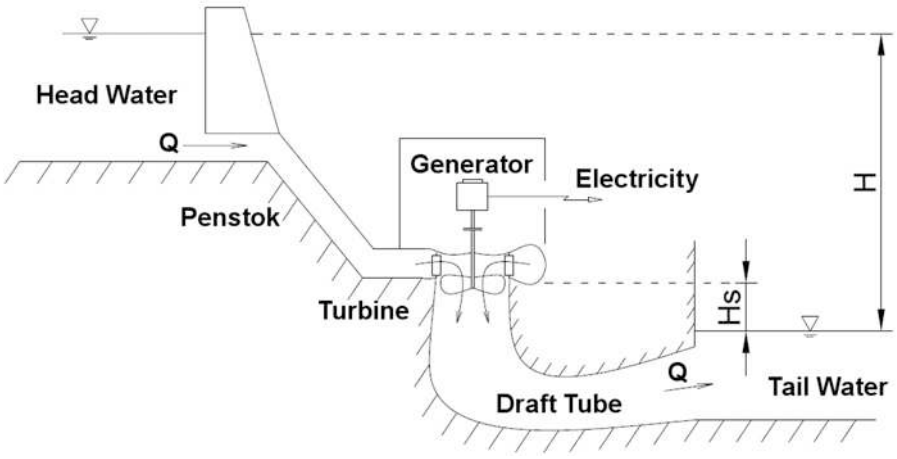

Fig. 1. Longitudinal cross-section view of hydraulic power plant

*Corresponding author. Tel.: +420 541 143 477, e-mail: y101274@stud.fme.vutbr.cz.

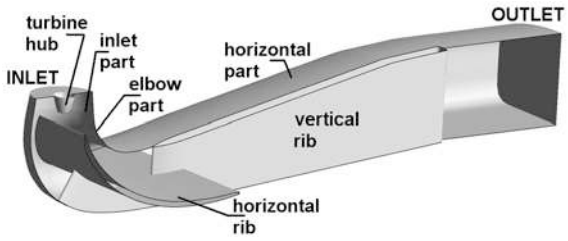

Fig. 2. Longitudinal cross-section view of DFT-A

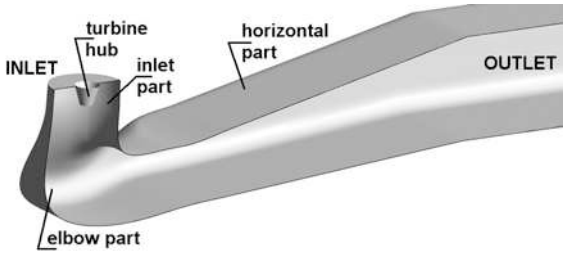

Fig. 3. Longitudinal cross-section view of DFT-B

Draft tube geometrical configuration A (DFT-A) – The elbow draft tube for vertical Kaplan turbine includes one horizontal rib (in elbow part) and one vertical rib (in horizontal part), Fig. 2. This draft tube is installed in hydro-power plant Střekov, Czech Republic.

Draft tube geometrical configuration B (DFT-B) – The elbow draft tube for vertical Kaplan turbine without any ribs, Fig. 3. This draft tube is result of shape modification of DFT-A for one specific velocity profile (different than velocity profile used in this work) [12].

Part of turbine runner hub (at the inlet of the draft tube), see Fig. 2 and Fig. 3, has been included and modelled as a stationary wall for both configurations of the draft tube.

The numerical computation has been carried out in commercial CFD software ANSYS FLUENT r.12. employing Reynolds Averaged Navier-Stokes equations to solve computational domain by finite volume method. We used Realizable $k-\varepsilon$ model of turbulence (RKE) with non-equilibrium wall function to perform steady state solution. The RKE model of turbulence and steady state of computation are chosen because of suitable capturing of flow properties and computational demands for evaluation, where dynamics properties of flow are not extracted. Each draft tube has been computed for a series of flow rates corresponding to operating regimes of the turbine. The best efficiency point of the turbine (100 % Q_{BEP}) corresponds to the mass flow $Q_m = 440$ kg/s. Inlet velocity profiles in Fig. 5 are the result of numerical computation of the new design of Kaplan turbine runner for hydro-power plant Střekov and data were obtained from ČKD Blansko Engineering.

Investigation of the three-dimensional separation, carried out by software ANSYS CFD-POST, and its influence on energy transformation is discussed. Skin friction lines, surface streamlines and critical points are used to identify the topological features of the flow.

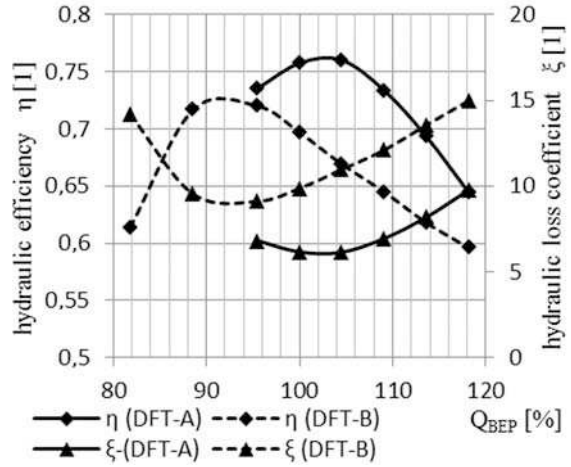

Fig. 4. Efficiency and hydraulic loss curves

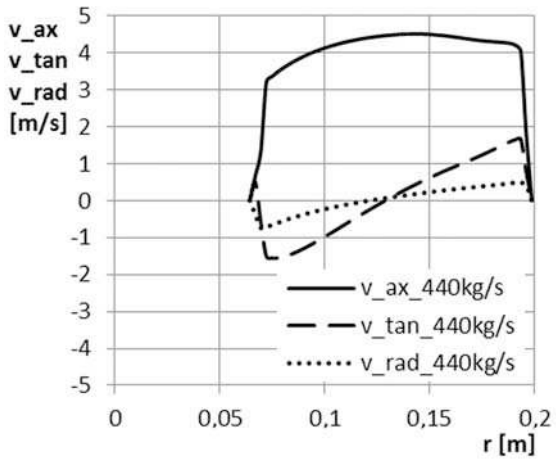

Fig. 5. Inlet velocity profile for CFD computation, flow rate 100 % Q_{BEP}

2. Energy transformation

The hydraulic efficiency (1), pressure recovery factor (2) and hydraulic loss coefficient (3) have been evaluated in several cross-sections for series of flow rates and swirl numbers

$$\eta = \frac{p_{s(2)} - p_{s(1)}}{p_{d(1)} - p_{d(2)}}, \tag{1}$$

$$c_p = \frac{p_{s(2)} - p_{s(1)}}{\frac{1}{2}\rho \bar{v}^2_{(1)}}, \tag{2}$$

$$\xi = \frac{2}{\bar{v}^2_{(2)}} \left[\left(\frac{\alpha_{(1)}\bar{v}^2_{(1)} - \alpha_{(2)}\bar{v}^2_{(2)}}{2} \right) + \frac{p_{s(1)} - p_{s(2)}}{\rho} \right], \tag{3}$$

where p_s is static pressure, p_d is dynamic pressure, $\bar{v}$ is mean velocity and α is Coriolis number. The number in parentheses represents $1 =$ inlet and $2 =$ outlet. The global development of these integral characteristics (1–3) is plotted in Fig. 6 for DFT-A and in Fig. 7 for DFT-B.

2.1. Energy transformation in DFT-A

Changes of DFT-A cross-sectional area are nearly linear from inlet to outlet of the draft tube. For flow rates 95.5 % Q_{BEP} and 100 % Q_{BEP} decrease of pressure recovery factor at the elbow part is observed and as will be shown in section 2.1, it is caused by flow separation under horizontal rib. For 109.1 % Q_{BEP}, the flow separation is significantly reduced, therefore, any considerable decrease of pressure recovery factor is not apparent.

The other decrease in pressure recovery factor is evident between cross-sections 9 and 11 for all three flow rates and is caused by the beginning of the vertical rib. The volume of vertical rib reduces cross-sectional area and thereby increases velocity and frictional losses. This effect is a consequence of the design so therefore it occurs for every flow rate. The smallest back-flow region at horizontal part of draft tube for whole range of flow rates is observed for 109.1 % Q_{BEP}. This is the reason for steeper slope of the pressure recovery curve than for other operating points. The highest value of DFT-A efficiency (1) is derived from efficiency curve plotted in Fig. 4 and corresponds to flow rate 103 % Q_{BEP}.

2.2. Energy transformation in DFT-B

The shape modification of DFT-B has had appreciable influence on the development of cross-sectional area at the elbow part of draft tube, see area between cross-section 3 and 6 in Fig. 7. The flow cross-section at the end of elbow part has been reduced because of separation risk on the inner curved wall. This modification was done for some past design of the draft tube with slightly different inlet velocity profile. It was anticipated that it might be beneficial also in combination with new runner design, which has to some degree altered outlet blade angles and hence also the outlet velocity components. Unfortunately, this assumption was not confirmed, flow inside the draft tube is rather sensitive to inlet boundary conditions and no positive impact for the DFT-B modification was observed.

DFT-B draft tube features rather steep increase of pressure recovery factor at the inlet part, which is connected with large wall divergence leading into reduction of velocity and abrupt transformation of kinetic energy into pressure energy. This is an undesirable effect, because too low kinetic energy of flow stream brings risk of flow separation at the downstream parts of the draft tube. In Fig. 13, it is shown that a large part of kinetic energy is dissipated just at the inlet part of draft tube and as will be shown in section 6.1, the flow separation occurs at the elbow

part of the draft tube. The highest value of DFT-B efficiency (1) is derived from efficiency curve plotted in Fig. 4 and corresponds to flow rate 92 % Q_{BEP}.

3. Back-flow regions

The back-flow regions block flow area, increase velocity and cause higher hydraulic losses.

DFT-A: The first significant back-flow region is situated under the horizontal rib and occupies right (for flow rate lower than that of the best efficiency point of turbine, Fig. 8) or left (for flow rate higher than that of the best efficiency point of turbine, Fig. 9) side of the draft tube. The highest suppression of this region is reached for flow rate 109.1 % Q_{BEP}, Fig. 10. The second back-flow region is situated on the top of horizontal part of the draft tube and is the most suppressed between operating points 104.5 % Q_{BEP} and 109.1 % Q_{BEP}. The highest hydraulic efficiency of DFT-A is reached for 103 % Q_{BEP} when the back flow regions are not the smallest. It shows influence of higher hydraulic losses caused by surface friction on the ribs when the flow rate increases.

DFT-B: Two back-flow regions occur. The first one is situated at the end of elbow part and second one at the horizontal part of draft tube. For flow rate 104.5 % Q_{BEP}, they are the largest and connected together, as shown in Fig. 10. The largest suppression of these regions is observed close to flow rate 95.5 % Q_{BEP}, Fig. 11.

4. Contours of dissipation

The dissipation function D for computation of turbulent flow by RANS equation is defined as follows

$$D = 2\iiint_V \left\{ (\mu+\mu_t) \left[\left(\frac{\partial v_x}{\partial x}\right)^2 + \frac{1}{2}\left(\frac{\partial v_x}{\partial y}+\frac{\partial v_y}{\partial x}\right)^2 + \frac{1}{2}\left(\frac{\partial v_x}{\partial z}+\frac{\partial v_z}{\partial x}\right)^2 + \left(\frac{\partial v_y}{\partial y}\right)^2 + \frac{1}{2}\left(\frac{\partial v_y}{\partial z}+\frac{\partial v_z}{\partial y}\right)^2 + \left(\frac{\partial v_z}{\partial z}\right)^2 \right] \right\} \mathrm{d}V\,. \tag{4}$$

For both draft tubes, the contours of dissipation (4) were computed at several cross-sections. Areas with the highest value of dissipation are coloured from black to white/vanish (over-range of colormap). The range of the colormap has been set and reduced so that only the dissipation inside of the volume is visible, because the highest value of dissipation occurs in boundary layer regions.

DFT-A: Several important areas with high value of dissipation are observed. The first one is at the inlet part of the draft tube. Considerable dissipation is caused by high velocity gradient of stream coming out from turbine runner. The second area is under the horizontal rib and corresponds with the back-flow region, compare Fig. 12 and Fig. 8. This result confirms that the back-flow regions are highly dissipative. The third area is located behind the trailing edge of the horizontal rib and is caused by sweeping of boundary layer into the main stream.

DFT-B: The main area of high dissipation is located close to the inner bend radius, Fig. 13. It is caused by very high velocity gradients induced by flow inside the elbow part. As in the case of DFT-A, significant dissipation caused by stream coming out from the turbine runner is observed at the inlet part of the draft tube.

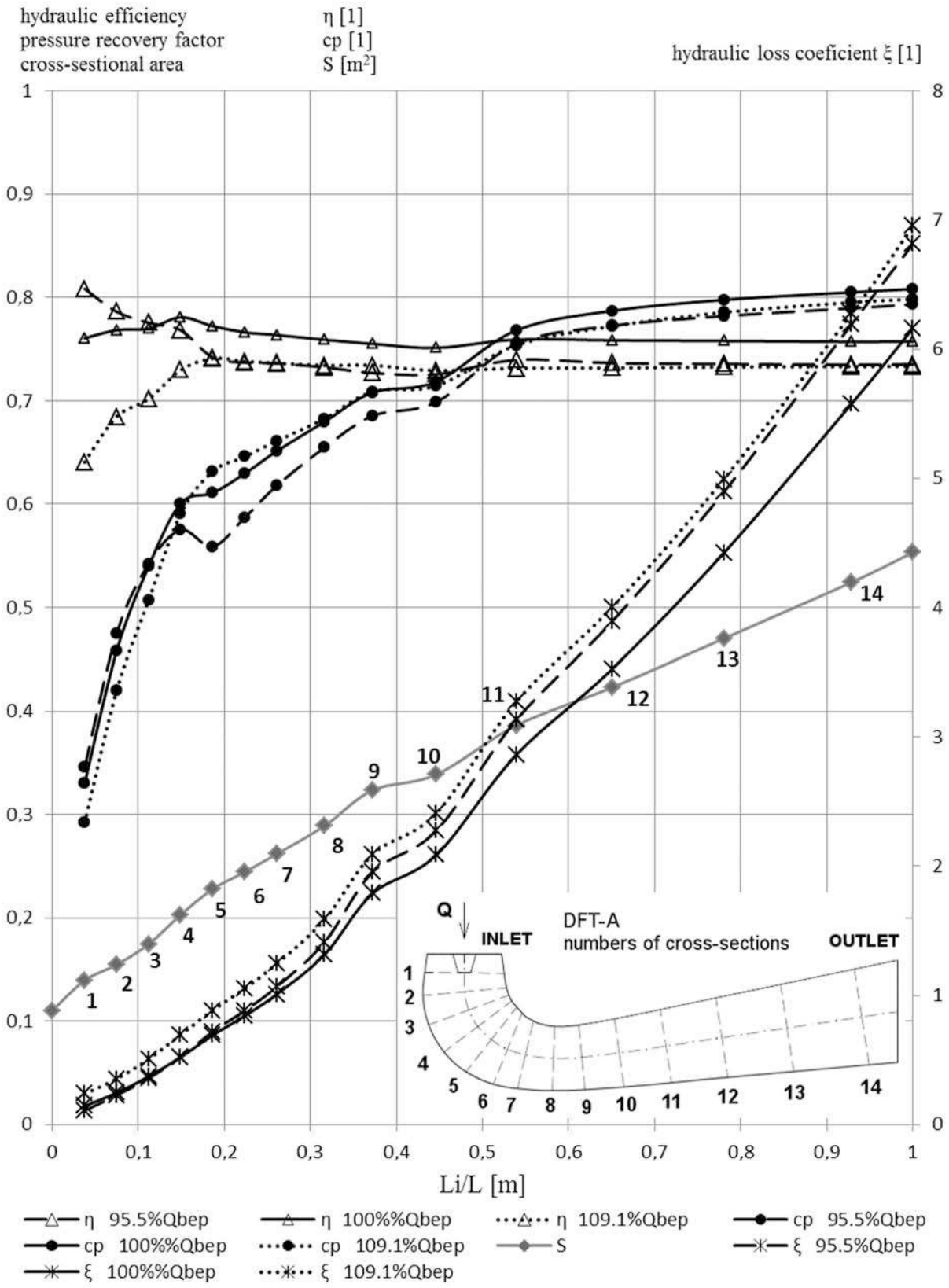

Fig. 6. Hydraulic efficiency, pressure recovery factor and loss coefficient evaluated in several cross-sections for three flow rates 95.5 % Q_{BEP}, 100 % Q_{BEP} and 109.1 % Q_{BEP} in case of DFT-A

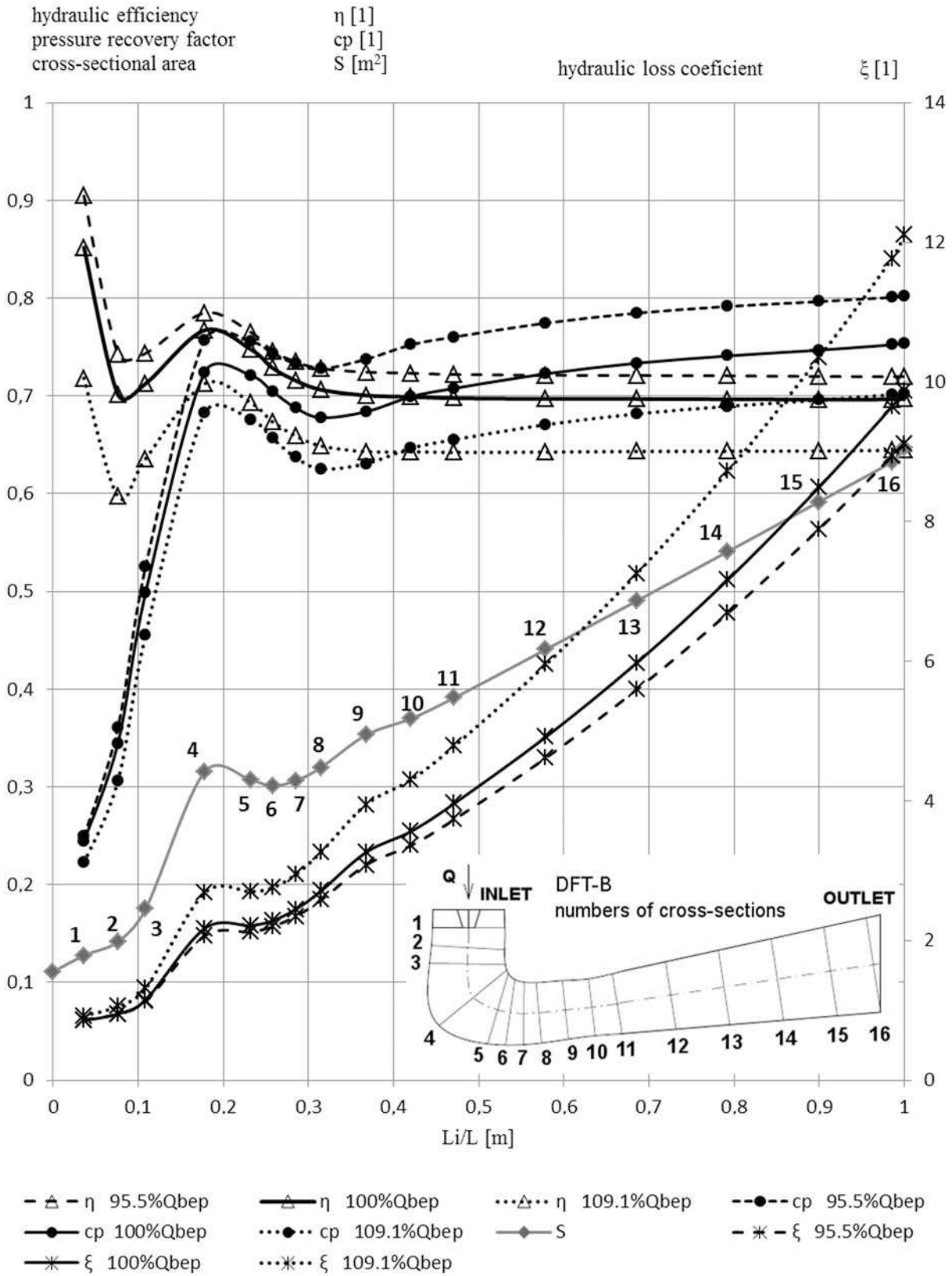

Fig. 7. Hydraulic efficiency, pressure recovery factor and loss coefficient evaluated in several cross-sections for three flow rates 95.5 % Q_{BEP}, 100 % Q_{BEP} and 109.1 % Q_{BEP} in case of DFT-B

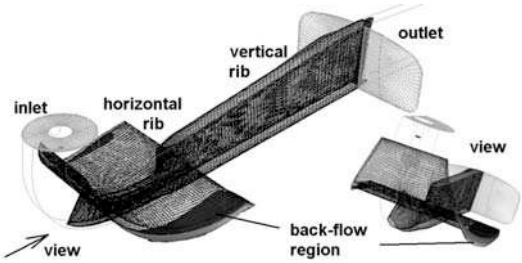

Fig. 8. Back-flow regions (in grey colour) in case of DFT-A, flow rate 104.5 % Q_{BEP}

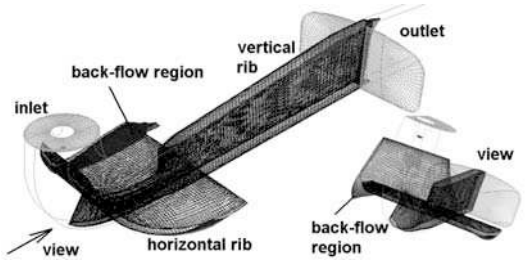

Fig. 9. Back-flow regions (in grey colour) in case of DFT-A, flow rate 109.1 % Q_{BEP}

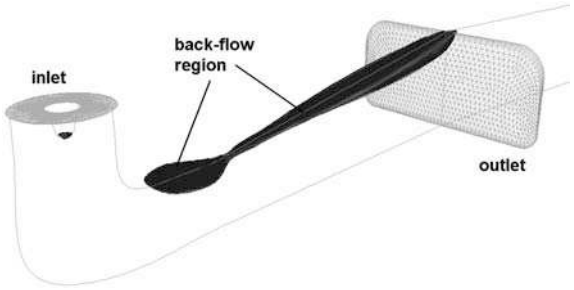

Fig. 10. Back-flow regions in case of DFT-B flow rate 104.5 % Q_{BEP}

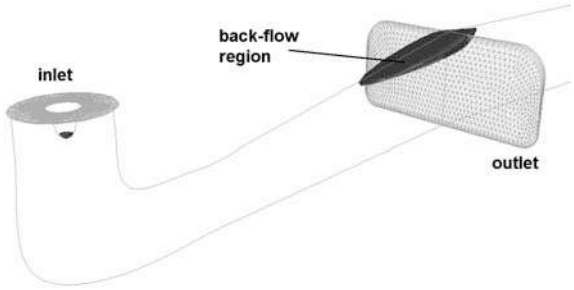

Fig. 11. Back-flow regions in case of DFT-B flow rate 95.5 % Q_{BEP}

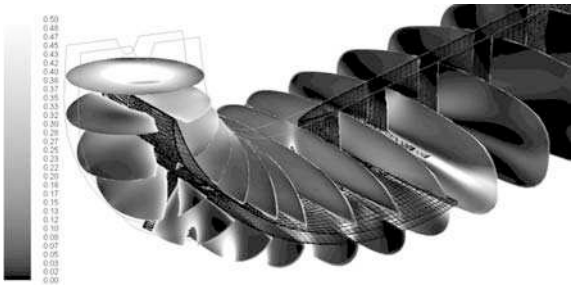

Fig. 12. Contours of dissipation in case of DFT-A

Fig. 13. Contours of dissipation in case of DFT-B

5. Topology of the three-dimensional separation

As mentioned in Tobak and Peak [13] and also in Depardon et al. [2], the hypothesis proposed by Legendre in 1956 brought a mathematical framework for description of the three-dimensional flow separation. The hypothesis is based on shear-stress patterns and critical points situated in the flow field and corresponding with the three-dimensional separated flow.

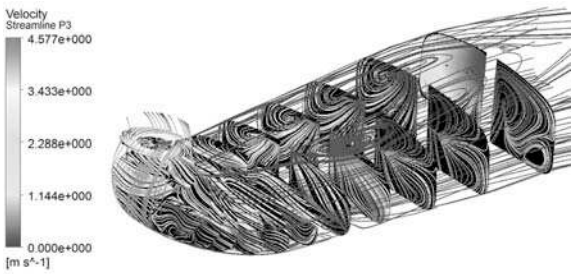

Fig. 14. Skin friction lines and surface streamlines in case of DFT-A

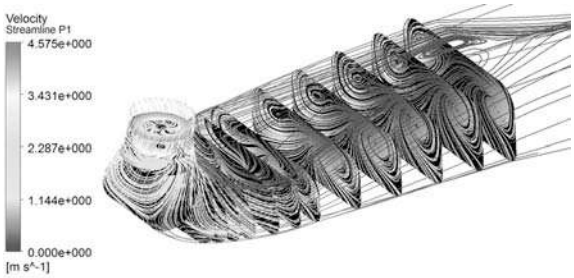

Fig. 15. Skin friction lines and surface streamlines in case of DFT-B

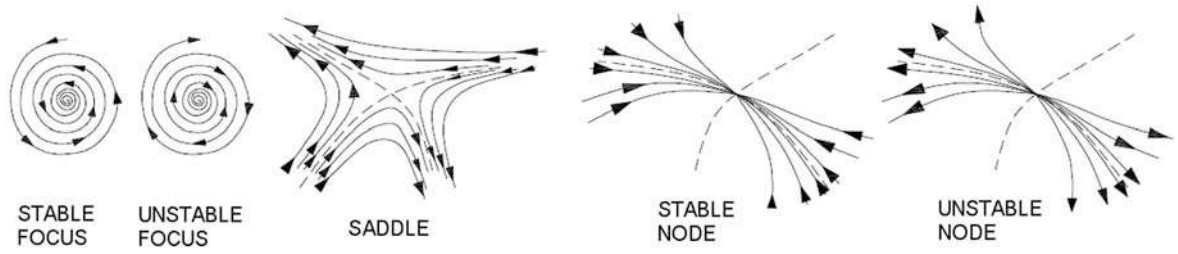

Fig. 16. Types of critical points

The three types of critical points in the flow field are identified, see Fig. 16. **Focus *F*** is a point where the vortex filament of the three-dimensional separation core is concentrated. Surface friction lines go into (stable) or out (unstable) of the centre of focus. **Saddle point *S*** is a place where surface friction lines converge from one side and diverge to the other side. **Node *N***: Surface friction lines go into (stable) or out (unstable) of the centre of node. Node usually lies near or directly onto solid surfaces.

For the exact determination of critical points in particular flow cross-section computation of velocity gradient tensor eigenvalue (5) is used [3, 4]

$$v_{ij}|_{x_{i,s}} = \begin{bmatrix} \frac{\partial v_x}{\partial x} & \frac{\partial v_x}{\partial y} \\ \frac{\partial v_y}{\partial x} & \frac{\partial v_y}{\partial y} \end{bmatrix} . \tag{5}$$

Each critical point (saddle, stable and unstable node, stable and unstable focus) is defined by sign of the eigenvalue of the tensor (5).

In case of elbow draft tube, several regions with risk of the three-dimensional separation occur. The beginning of the three-dimensional flow separation lies onto draft tube body surface where boundary layer separates and is carried out by main stream. The vortex region originates from this separation and causes blockage effect leading to the flow acceleration.

Exact visualization and evolution of separation core (so-called dividing surface) in flow field is rather difficult, especially when dealing with 3D data. One of the possibilities is to use the Sujudi-Haimes algorithm [9]. The computational algorithm looks for the points in the velocity field where a single real eigenvector exists and this is parallel to the velocity vector [5, 6]. There are also other approaches to visualize separation surfaces emanating from critical points, see [7, 10]. Some of them are specifically focused on swirling flows, see [1].

In this work, prediction of the core evolution is solved only by visualization method based on searching of foci in particular draft tube cross-sections (surface streamlines) and on the solid surfaces (skin friction lines), Fig. 14 and Fig. 15. This method is simplification of finding possible occurrence of core but not very suitable for tracking the spatial evolution of the core. Setting the cross-section orientation represents a very difficult task, because foci are properly visible only on cross-section which is almost exactly perpendicular to the separation core. It is also advised to observe back-flow regions, which are related to global flow separation and lead to the hydraulic efficiency drop.

5.1. Global flow separation

In case of elbow diffusers, the main part with risk of the three-dimensional separation is the bend. For rectangular curved diffuser, the authors of [8] investigated three kinds of global flow separations: *massive*, *typical* and *simple*. The typical idea of global flow separation: “The global flow separation begins, where the flow is separated from the wall and formed the back-

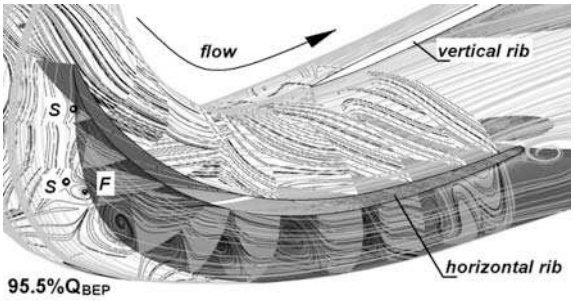

Fig. 17. Right view on elbow part of DFT-A for flow rate 95.5 % Q_{BEP}

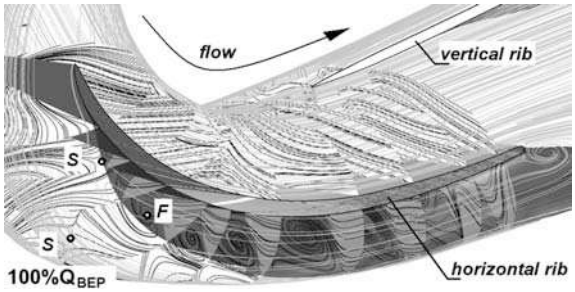

Fig. 18. Right view on elbow part of DFT-A for flow rate 100 % Q_{BEP}

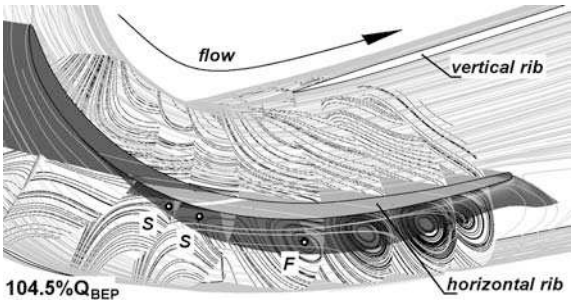

Fig. 19. Right view on elbow part of DFT-A for flow rate 104.5 % Q_{BEP}

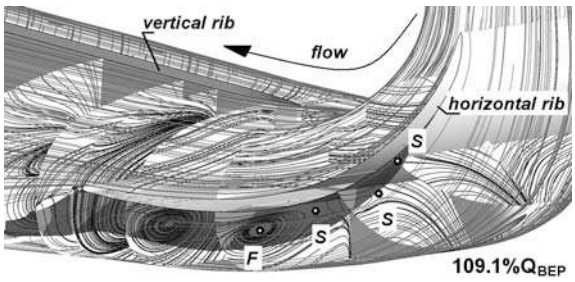

Fig. 20. Left view on elbow part of DFT-A for flow rate 109.1 % Q_{BEP}

flow regions" is stated in [8]. The global flow separation is highly dissipative phenomenon, increases hydraulic losses and reduces hydraulic efficiency.

In case of turbulent flow in the draft tube (unsteady, three-dimensional with rotational character), the flow topology of the separation is very complex and directly corresponds with shape of the draft tube. This statement is especially characteristic of the draft tube containing ribs. Types of the three-dimensional separation corresponding to each of the investigated draft tubes will be shown in sections 5 and 6.

5.2. Local flow separation

In contrary to the case of global flow separation, the local flow separation is not related to back-flow regions. Hence no significant negative effect, as lower efficiency due to higher dissipation, has been documented. The example of local type of three-dimensional separation is observed in section 5.2 for the DFT-A draft tube.

6. Three-dimensional separation in DFT-A draft tube

6.1. Separation under horizontal rib

This separation is mainly caused by leading edge of horizontal rib which suppresses stream rotation at the inlet of the draft tube. This separation is in combination with back-flow region that means it is the global flow separation which decreases energy transformation and deteriorates efficiency.

Flow rate: (Figs. 17–20)

- **95.5 % Q_{BEP}:** The back-flow region is very large and starts from leading edge of the horizontal rib, see Fig. 17, and develops downstream to the draft tube. The global flow separation is represented by saddle point S in combination with focus F.

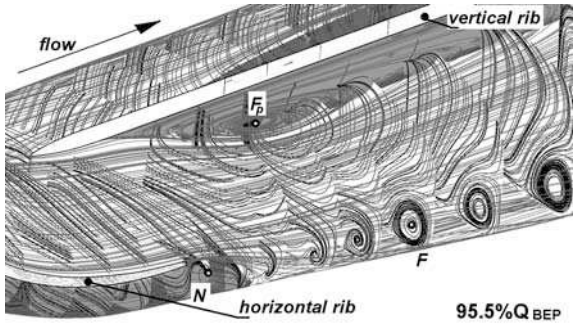

Fig. 21. Right view on horizontal part of DFT-A for flow rate 95.5 % Q_{BEP}

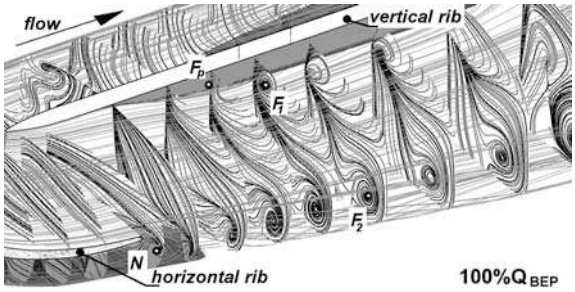

Fig. 22. Right view on horizontal part of DFT-A for flow rate 100 % Q_{BEP}

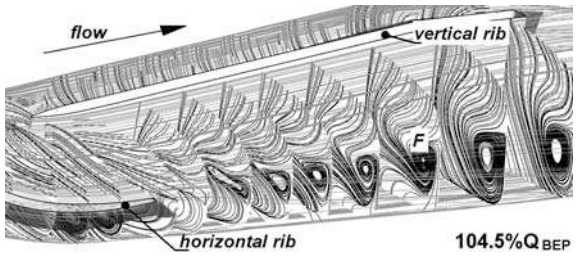

Fig. 23. Right view on horizontal part of DFT-A for flow rate 104.5 % Q_{BEP}

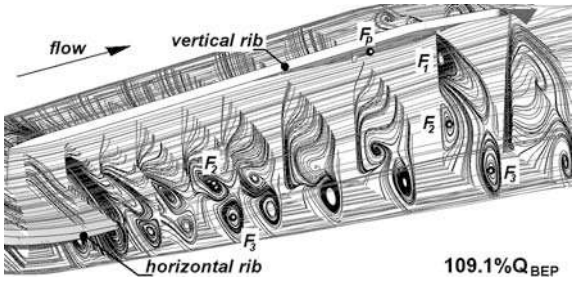

Fig. 24. Right view on horizontal part of DFT-A for flow rate 109.1 % Q_{BEP}

- **100 %** Q_{BEP}**:** The back-flow region and global flow separation are smaller by getting closer to the best efficiency point of the draft tube, see Fig. 18.
- **104.5 %** Q_{BEP}**:** This flow rate is close to the best efficiency point. The global flow separation is considerably reduced but still observed, see Fig. 19.

6.2. Separation at horizontal part of draft tube

The global and the local types of flow separation occur at the horizontal part of draft tube. The global flow separation with large back-flow region is observed for higher and lower flow rates out from the best efficiency point. The local flow separation is caused by boundary layers sweeping from trailing edge of horizontal rib. These boundary layers are then carried out by main stream and formed into separation core.

Flow rate: (Figs. 21–24)

- **95.5 %** Q_{BEP}**:** The large back-flow area surrounds the top of vertical rib. The global flow separation starts in F_p onto roof of draft tube body and winds into main stream. The local flow separation is represented by node N and focus F, Fig. 21.
- **100 %** Q_{BEP}**:** The separation with beginning in F_p is smaller than previous one but still considerable back-flow region occurs. Separation core in Fig. 22 is wound through the focus F_1. Node N and focus F_2 represent the local flow separation.
- **104.5 %** Q_{BEP}**:** This flow rate is close to the best efficiency point of the draft tube. The global flow separation in Fig. 23 is almost reduced. On the other hand, the local flow separation with core in focus F is getting stronger.
- **109.1 %** Q_{BEP}**:** High extensive local flow separation with two cores goes through the foci F_2 and F_3 as seen in Fig. 24. The small global flow separation with beginning in F_p and separation core going through F_1 is located near the top of vertical rib.

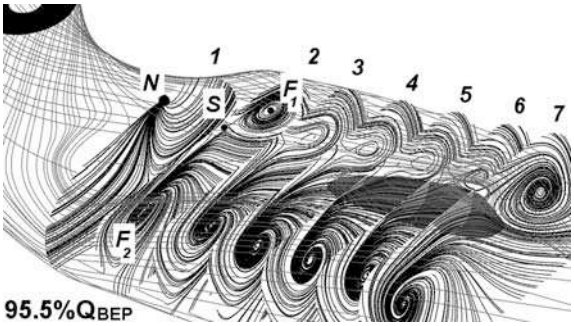

Fig. 25. Top view on DFT-B, flow rate 95.5 % Q_{BEP}

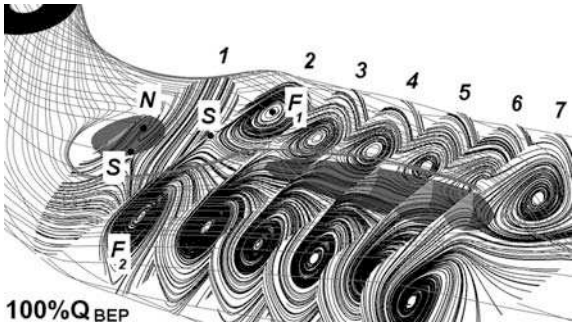

Fig. 26. Top view on DFT-B, flow rate 100 % Q_{BEP}

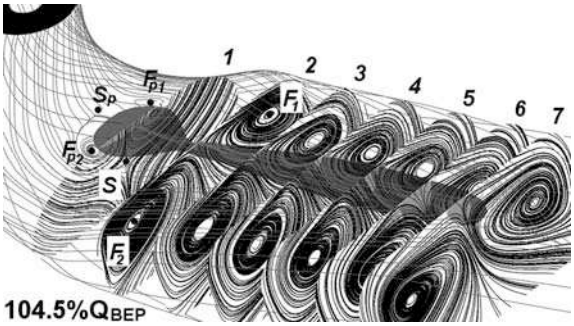

Fig. 27. Top view on DFT-B, flow rate 104.5 % Q_{BEP}

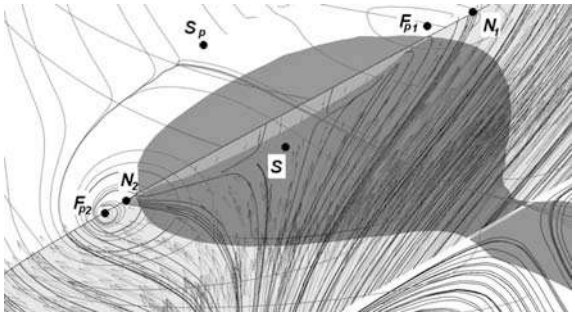

Fig. 28. Detailed view on global flow separation beginning, flow rate 104.5 % Q_{BEP}

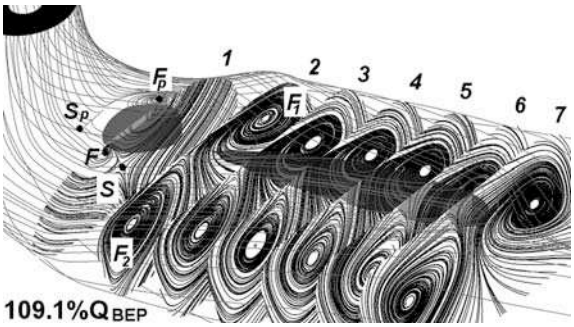

Fig. 29. Top view on DFT-B, flow rate 109.1 % Q_{BEP}

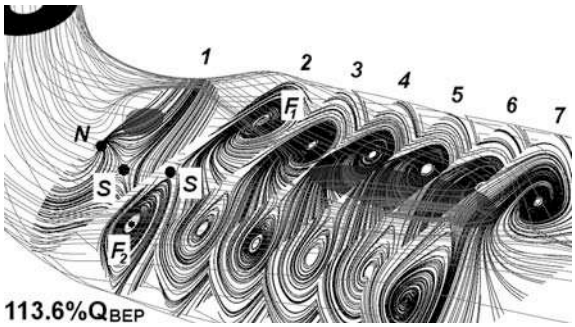

Fig. 30. Top view on DFT-B, flow rate 113.6 % Q_{BEP}

Only the right channel of horizontal part is shown for demonstration. The same kinds of the three-dimensional separations occur also in the left channel.

7. Three-dimensional separation in DFT-B draft tube

The main region of elbow draft tube (without ribs) where could be formed the three-dimensional separated flow is at the inner radius of the bend.

7.1. Separation at the end of elbow part of draft tube

Flow rate: (Figs. 25–30)

- **95.5 % Q_{BEP}:** The unstable node N in combination with saddle S forms the beginning of separation. The back-flow region is very small and is situated far away from separation beginning. Hence this separation should be local type of separation, see Fig. 25.

- **100 % Q_{BEP}:** The unstable node N in combination with saddle S forms the beginning of global flow separation because the small back-flow region is formed at the end of elbow part, see Fig. 26.
- **104.5 % Q_{BEP}:** The beginning of large global flow separation is represented by combination of saddle S_p with foci F_{p1} and F_{p2} on solid surface. From these foci separation cores start, which go through foci F_1 and F_2 situated in flow cross sections 2–7, see Fig. 27 and Fig. 28.
- **109.1 % Q_{BEP}:** The global flow separation is still extensive, but diminishes and only one focus F_p on draft tube body occurs in Fig. 29.
- **113.6 % Q_{BEP}:** The flow topology in Fig. 30 is similar to the flow rate 100 % Q_{BEP} as shown in Fig. 26. At the end of elbow part is formed the small back-flow region which leads to global flow separation.

The detailed view on the beginning of global-flow separation for flow rate 104.5 % Q_{BEP} is shown in Fig. 28. The two separation cores start in foci F_{p1} and F_{p2}, which are in combination with saddle S_p. Nodes N_1 and N_2 and saddle S characterize the separation in flow cross-section.

8. Swirling flow

The swirling flow at the draft tube inlet is mainly caused by tangential velocity of stream exiting from the turbine runner. The swirl number S_n [11] is used for description of the swirling flow

$$S_n = \frac{\int v_{ax} v_{tan} r \, \mathrm{d}S}{R \int v_{ax}^2 \, \mathrm{d}S}, \tag{6}$$

where v_{ax} is axial velocity, v_{tan} is tangential velocity, r is radial coordinate and R is inlet radius of the draft tube. The swirl numbers computed by (6) in the inlet cross-section are plotted in Fig. 31. It can be seen that from flow rate 104.5 % Q_{BEP} to higher the flow rotates in opposite direction than turbine runner. Fig. 32 shows hydraulic efficiency curves for each draft tube against values of the swirl numbers. The best efficiency point for DFT-A is obtained for lower swirl number than in the case of DFT-B. This difference shows the significant influence of horizontal guide rib on flow in draft tube in relation to global flow separation caused by this rib. Result for DFT-A indicate that low swirling flow at the inlet of the draft tube is important

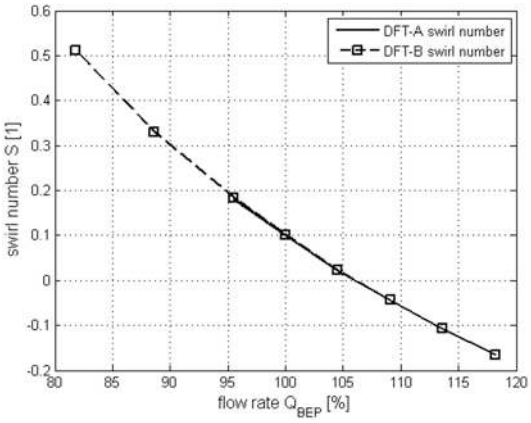

Fig. 31. Swirl number S_n versus flow rate Q_m

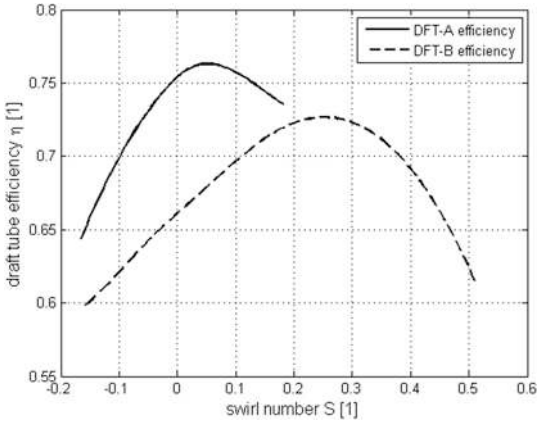

Fig. 32. Draft tube efficiency η vs. swirl number S_n

for smoother splitting of water stream by leading edge of the horizontal rib. Guide rib acts like inhibition for swirling flow exiting from the runner. Thus, for the highest or lowest value of the swirl number, the back-flow region situated under horizontal rib and three-dimensional separation grows as well. On the other hand, the higher swirling flow with positive value of swirl number (the swirl rotates in same direction as turbine runner) is required for flow rate corresponding with the best efficiency point of DFT-B. Higher swirling flow pushes the boundary layer against the walls, which reduces the risk of separation mainly in the elbow part of draft tube.

9. Conclusion

The main result of this work is referring to the global flow separation influence on the draft tube efficiency. The global flow separation in combination with the back-flow regions is a highly dissipative phenomenon. When flow rate moves out of the best efficiency point of the draft tube, then extension of the global flow separation is observed for both draft tubes. Insignificant role on draft tube efficiency is also hydraulic losses caused by surface friction, mainly in case of DFT-A with two ribs.

The efficiency maximum of DFT-A is obtained for flow rate 103 % Q_{BEP} and swirl number $S_n = 0.05$. The global flow separation is the most considerably reduced between flow rates 104.5 % Q_{BEP} and 109.1 % Q_{BEP} and for swirl number close to $S_n = 0$. These results show compromise between frictional losses which grow with increasing flow rate, and non-swirling flow ensuring the lowest three-dimensional separation. But this relation is only valid for case of DFT-A or the similar elbow draft tubes with guide rib.

In case of DFT-B the swirl flow does not have undesirable effect, on the contrary the swirling flow with $S_n = 0.25$ in the best efficiency point of draft tube prevents risk of separation. It is seen that for flow rate 104.5 % Q_{BEP} and $S_n = 0$ the largest global flow separation is reached with important influence on the draft tube efficiency. This separation is in large amount caused by non-swirling flow.

It is difficult to describe exact character of the local type of flow separation in draft tubes because it does not correspond with back-flow regions. Thus, it becomes difficult to predict evolution of separation core. Present investigation indicates that local type of flow separation has no evident influence on the draft tube efficiency.

The results of the flow topology confirm that the patterns of skin friction lines onto solid surfaces are good indicators for quality of flow in particular region of the flow field. Identification of the skin friction patterns is rather sensitive tool to observe flow variations in the draft tube interior, if the inlet velocity profile is changed. In other words skin friction lines enable convenient observation how design modifications are reflected in flow topology. Combining the information about details of the flow field with integral parameters like hydraulic efficiency or loss coefficient, it offers full picture enabling optimization of the draft tube shape or the runner blade outlet angles.

Acknowledgements

Authors gratefully acknowledge support of the research by Czech Science Foundation under project No. 101/09/1715 “Cavitating vortical structures induced by rotation of liquid” and by Ministry of Trade and Industry under project No. 2A-1TP1/108 “Performance increase and operational range broadening for upgraded low head hydraulic power plants”.

References

[1] Bisgaard, A. W., Structures and bifurcations in fluid flows with application to vortex breakdown and wakes, Ph.D. thesis, Technical University of Denmark, Kongens Lyngby, 2005.

[2] Depardon, S., Lasserre, J. J., Boueilh, J. C., Brizzi, L. E., Borée, J., Skin friction pattern analysis using near-wall PIV, Experiments in Fluids 39 (2005) 805–818.

[3] Helman, J., Hesselink, L., Representation and display of vector field topology in fluid flow data sets, Computer 22(8) (1989) 27–36.

[4] Kenwright, D. N., Henze, C., Levit, C., Feature extraction of separation and attachment lines, IEEE transactions on Visualization and Computer Graphics 5(2) (1999) 135–144.

[5] Mauri, S., Kueny, J. L., Avellan, F., Werlé-Legendre separation in a hydraulic machine draft tube, Journal of Fluids Engineering 126 (2004) 976–980.

[6] Mauri, S., Numerical simulation and flow analysis of an elbow diffuser, Ph.D. thesis, EPFL Lausane, 2002.

[7] Peikert, R., Sadlo, F., Topologically relevant stream surfaces for flow visualization, Proceedings of the Spring Conference on Computer Graphics, Budmerice, Slovakia, 2009, pp. 43–50.

[8] Sedlář, M., Příhoda, J., Investigation of flow phenomena in curved channels of rectangular cross-section, Engineering Mechanics 14 (2007) 387–397.

[9] Sujudi, D., Haimes, R., Identification of swirling flow in 3-D vector fields. Department of Aeronautics and Astronautics Massachusetts Institute of Technology Cambridge, MA 02139, pp. 1–8.

[10] Surana, A., Jacobs, G. B., Haller, G., Extraction of separation and attachment surfaces from three-dimensional steady shear flows, AIAA Journal 45(6) (2007) 1 290–1 302.

[11] Susan-Resiga, R., Ciocan, G. D., Anton, I., Avellan, F., Analysis of the swirling flow downstream a Francis turbine runner, Journal of Fluids Engineering 128 (2006) 177–189.

[12] Svozil, J., Rudolf, P., Kaplan turbine draft tube optimization, Research report VUT-EU13303-QR-01-10, Brno, 2010. (in Czech)

[13] Tobak, M., Peake, D. J., Topology of three-dimensional separated flows, Annual Review of Fluid Mechanics 14 (1982) 61–85.